TIMED Doppler Interferometer (TIDI) Observations of Migrating Diurnal and Semi-diurnal Tides

Qian Wu[1], T. L. Killeen[1], D. A. Ortland[2], S. C. Solomon[1],
R. D. Gablehouse[1], R. M. Johnson[1], W. R. Skinner[3], R. J. Niciejewski[3], S. J. Franke[4]

[1]High Altitude Observatory
National Center for Atmospheric Research
P. O. Box 3000
Boulder, CO 80307-3000

[2]Northwest Research Associates
P. O. Box 3027
Bellevue, WA 98009-3027

[3]Space Physics Research Laboratory
The University of Michigan
2455 Hayward St.
Ann Arbor, MI 48109-2143

[4]Department of Electrical and Computer Engineering
University of Illinois
Urbana, IL 61802

Abstract

Based on zonally averaged TIDI meridional wind data from one yaw period (2004 03/19 – 05/19) near equinox, we examine the latitudinal and altitudinal distribution of the migrating diurnal and semi-diurnal tides using least squares fitting method to provide a global view of these tidal waves. The TIDI results are compared with Global Scale Wave Model 00 output for the month of April. The diurnal tide amplitude distribution and are in a good agreement in the northern hemisphere and differ in amplitude in the southern hemisphere. The TIDI results show a lower peak altitude (97 km) while GSWM00 peaks at 102 km. The vertical wavelength from the TIDI is about 20 km while the model predicts 25 km. The semi-diurnal tide comparisons are also reasonable. Both model and TIDI data show peak amplitudes at 45° latitude. The TIDI meridional winds are comparable with ground based meteor radar measurements at Maui.

Introduction

Migrating tides are the most prominent features in the mesosphere and lower thermosphere (MLT) region. Understanding tidal wave generation, propagation, and interactions with gravity waves and planetary waves is the key to the insight of the dynamics and energetics of the MLT region. There is a long history of tidal wave study starting with the classical tidal theory (e.g., Chapman and Lindzen, 1970). Tides are also affected by advection, background mean neutral winds, nonlinear interaction between different tidal modes, and the geographic distribution of latent heat release. Various numerical tidal models have been

developed to simulate these effects (e.g, Forbes, 1982a,b; Vial 1989; Forbes and Hagan, 1988; Hagan et al., 1995; Hagan and Roble, 2001; Hagan and Forbes, 2002; 2003).

Early observations of MLT tides were made by ground based instruments (Fabry-Perot interferometer, lidar, meteor radar, MF radar, and incoherent scatter radar) and rockets. Since tides are global scale waves, it is impossible for observations from a single ground station to provide an overall picture of the wave. Therefore, multiple-station observations are often used to examine tides. One example of such an effort is the PSMOS (Planetary Scale Meospause Observing System) project, in which many investigators participated using ground-based radars around the world (e.g., Pancheva et al., 2002). These observations have revealed a great deal about various tidal modes in the MLT region. Nevertheless, the deployment of ground-based instruments is limited by the geography, because 70% of the Earth's surface is covered by ocean. The usage of multiple instrument data sets also raises the issue of inter-instrument calibration.

The introduction of satellite observations of mesosphere and lower thermosphere neutral wind brought a new perspective to the study of upper atmosphere tides, because satellite observations can provide near-global coverage. The Upper Atmospheric Research Satellite (UARS) High Resolution Doppler Interferometer (Hays et al., 1993) and Wind Imaging Interferometer (Shepherd et al., 1993) have provided a much better global view of tides. Migrating tides were studied based on data sets from these two instruments (Morton et al., 1993; Lieberman and Hays, 1994; Hays et al., 1994; Burrage et al., 1995a; Burrage et al., 1995b; McLandress et al., 1996; Khattatov et al., 1997a; b; Huang and Reber, 2003). Yet UARS observations did not provide coverage over high latitude regions, because of its orbital inclination. Moreover HRDI provided only single altitude (at 95 km) observation on the nightside. Consequently, the tidal analysis was hampered somewhat by the limited local time and altitude coverages.

To provide a better pole-to-pole coverage for the study of the MLT dynamics and energetics, on December 7, 2001, TIMED (Thermosphere Ionosphere Mesosphere Energetics and Dynamics) satellite was launched into orbit. TIMED is a two-year mission sponsored by NASA to study the mesosphere and lower thermosphere, which provide a crucial link between solar activity and the Earth. The satellite is in a near circular orbit with 625 km altitude, 74.1° inclination, and a 3° per day precession rate. Approximately every 60 days, a 180° yaw maneuver of the satellite is performed to avoid the sunlight shining onto the cold side of the spacecraft. There are four instruments onboard the TIMED satellite: TIMED Doppler Interferometer (TIDI), Global Ultraviolet Imager (GUVI), Sounding of the Atmospheric Using Broadband Emission Radiometry (SABER), Solar Extreme ultraviolet Experiment (SEE). TIDI was designed to measure the neutral winds in the mesosphere and lower thermosphere. In this report, we describe the TIDI measurements of the migrating diurnal and semi-diurnal tides in the MLT meridional winds. Meridional winds were chosen, because their small background winds and strong tidal features. This paper is organized as follows: We briefly describe the instrument in the next section and followed by descriptions of TIDI data analysis method and results. Comparisons with Global Scale Wave Model (GSWM00) output and ground based meteor radar measurements are presented. Finally we summarize our findings.

Instrument

The TIDI instrument was developed and built by the University of Michigan (Killeen et al, 1999). TIDI measures neutral winds by performing limb scans of various upper atmosphere airglow layers and monitoring the Doppler shift of airglow emissions induced by neutral winds. It traces its roots to earlier Fabry-Perot interferometers onboard satellites such as Dynamic Explorer 2 (Hays et al., 1981; Killeen and Hays, 1982) and UARS (Hays et al., 1993). TIDI is a more sensitive instrument with four telescopes, a circle to line interferometer (CLIO) conical mirror, and a CCD detector with quantum efficiency exceeding 60% at some wavelengths. One reason for the high sensitivity is due to the multiplexing

advantage of the simultaneous recording of spectra from all four telescopes. The CLIO further reduces the readout noise of the CCD by removing the need to sample individual pixels (Hays, 1990).

The four TIDI telescopes are orthogonally oriented, allowing the instrument to measure neutral wind vectors on both sides of the satellite track. The two telescopes viewing the same side of the track observe the same locations with a time delay of 9 minutes as the spacecraft moves forward. The viewing directions of these two telescopes are perpendicular to one another. Assuming that the neutral winds do not change much during the short time period, then the samplings at the two directions can be used to form the neutral wind vector in terms of the meridional and zonal components.

The local time coverage on day 2004080 (03/20) is shown in Figure 1. There are four local time samplings at latitudes equatorward of ±60° and two at latitudes poleward of ±60°. The local time coverage pattern shifts slowly (by 0.2 hr/day) towards earlier local times as time progresses. The satellite orbits the Earth 15 times (98 minutes per orbit), and the local time of the orbit will not change much within a day. As the Earth rotates under the TIMED orbit, TIDI provides longitudinal coverage around the globe. The single black arrow indicates the flight direction of the satellite. The two-head arrows mark the hemispheres where the coldside (southern) or warmside (northern) samplings provide equator to pole coverage with similar local times. The four telescopes scan the O_2 (0-0) airglow emissions P9 line in a repeating sequence called a scan cycle, which defines the operational mode. TIDI has both daytime and nighttime operational modes. Typical day and nighttime operational modes of TIDI take about 105 seconds to complete and TIDI repeats the same scan pattern until the spacecraft crosses the day/night boundary. The 100 seconds temporal resolution translates to about 7° latitudinal grid for spatial coverage. The TIDI daytime coverage extends from 70 km to 115 km. The nighttime coverage is narrower (between 80 and 105 km) due to the more limited altitude range of nightglow emissions.

TIDI Data Analysis

The data processing procedure comprises three stages. In the first stage, the TIDI spectral data are merged with spacecraft orbital information to form Level 1 spectral data. The spectral data are processed to remove the various backgrounds and then normalized to physical units of Rayleigh/cm^{-1} for each spectral channel. Line-of-sight winds are computed without any inversion algorithm. In the second stage, the spectral data are inverted in altitude to form line-of-sight inverted winds (Level 2 data). In the final stage, the inverted line-of-sight winds from different telescopes are combined to form neutral wind vectors in terms of meridional and zonal components (Level 3).

TIDI experienced some anomalies after the launch, namely the ice buildup on instrument optical surfaces and higher than expected background (Skinner et al., 2003). The ice buildup on optical surface caused a strong cross-talk between telescope fields and a reduction in the instrument throughput. Fortunately, the ice buildup has been reduced by two roll maneuvers, during which the satellite coldside was tilted towards the warmer Earth surface and away from the much colder deep space. Consequently, the instrument was warmed up to allow ice to sublimate. The cause of the high background is likely due to the leak on the back of the instrument, which allows the Earth's reflection of the sunlight to enter the instrument and registered on the instrument detector. The cause for the high background was later confirmed by the close resemblance between the background intensity map and cloud cover pattern on the Earth's surface (Skinner et al. 2003). To remove the highly varying background, TIDI periodically samples backgrounds, which are represented in terms of Empirical Orthogonal Functions (EOF). The EOFs are calculated from a large collection of background samples. The backgrounds for spectral data between background samples are estimated by interpolation of the amplitudes of the EOF of the measured backgrounds according to the data sampling times. These procedures have been implemented into the daily data production software.

The zonally averaged meridional wind data taken on day 2004080 (03/20) are shown in Figure 2. The zonal average is performed on a 5° degree satellite track angle grid. The two panels show the meridional winds from the coldside (left panel) and warmside (right panel). Within each panel, the neutral winds from the ascending (left) and descending (right) nodes are plotted. On this day, the ascending node is on the nightside, as indicated by the narrower altitude range and descending node is on the dayside. Because of the relatively slow precession rate (3° per day), measurements from 15 orbits during a day are at about the same local times. Hence, zonally averaging the 15 orbits can reduce non-migrating tide contributions and enhance the migrating tides, because migrating tides are longitudinally independent. The errors for the averaged wind are about 15 m/s between 90 and 100 km altitudes. The meridional winds in Figure 2 show clear signs of the migrating diurnal tide with its anti-symmetric wind pattern about the equator. The vertical feature also indicates the vertical wavelength of the migrating diurnal tides is about 20 km. In this study we use portions of the satellite samplings marked by those arrows on both the coldside (southern hemisphere) and warmside (northern hemisphere) to extract the migrating diurnal and semi-diurnal tides. These segments of the measurements are also highlighted in Figure 1. We used these segments because they provide similar local time coverage from the equator to the pole in each of the hemisphere. We combined the data from a complete yaw period from date 2004/03/19 to 2004/05/19. Hence, we have complete 24-hour local time coverage from 60-day of observation. We selected this yaw period because this is a period near equinox, when the migrating diurnal tide tends to be strong (Hays et al., 1994). Figure 3 shows the meridional winds from three latitudes in the northern hemisphere based on observations during this yaw period. The neutral winds at 11.29° N (the upper panel) show prominent positive and negative bands with a slope of local time variation consistent with a diurnal tide. The neutral winds at 30.35° N (the middle panel) also show strong diurnal tide, however, the tilt is slightly steeper probably due to the influence of the semidiurnal tide. The neutral winds at 44.79° N are shown in the lower panel and the neutral winds contains mainly the semidiurnal tide as indicated by the a negative and positive phase within 12 hour during the daytime hours (6 – 18 LT).

Assuming that the tidal amplitude and phase did not change dramatically during this time period, we perform least squares fits to the meridional wind data from this yaw period at different latitudes and altitudes with a background wind, a diurnal oscillation, and a semidiurnal oscillation to extract the migrating diurnal and semidiurnal tide parameters. In this way, we can estimate the latitudinal and altitude distribution of the migrating diurnal and semi-diurnal tides without assuming any composition of tidal modes. This method, however, has several drawbacks. First, the tidal amplitude may not be constant over the 60 days, hence this is an averaged result. Second the mean winds may also change during the yaw period and introducing additional day-to-day variations, which are treated as local time variation in our analysis. Since the diurnal tidal amplitude is so large during equinox, these variations should not affect the final results significantly. We should note that twilight data from the coldside near 6 and 18 LT were removed before the analysis because of limb scan data inversion difficulty.

Figure 4 shows the least square fitting results for the diurnal and semidiurnal tides. The northern hemisphere is from the warmside and southern from the coldside. The upper left panel is for the diurnal tide amplitude and lower left is for the diurnal tide phase. Near the equator the diurnal tide amplitude forms a butterfly pattern, while the phases are nearly 180° off between the two hemispheres. The peak amplitude in the northern hemisphere is about 70 m/s between 95 and 100 km. The amplitude is about 40 m/s in the southern hemisphere. The error for the amplitude at these peaks are about 5 m/s and phase errors are about 0.2 hour. It should be pointed out the uncertainties in amplitude does not include contributions from the day-to-day variation in the tidal amplitude and background winds. Compared to the symmetric diurnal tide (1,1) mode pattern, the TIDI results are strongly asymmetric. A close examination of the Figure 2 also reveals that the amplitude is stronger in the northern hemisphere than in the southern hemisphere. The asymmetry could be due to contributions from other tidal modes. Twilight data at southern high latitudes (higher than -70° S) were removed due to poor data quality.

It should be noted that the diurnal tide amplitude during the equinox is similar to what was observed by UARS HRDI (Hays et al, 1994, Burrage et al, 1995). While we are more focused on latitudinal and altitudinal variation of the diurnal tide, the HRDI analysis was more concerned about the daily variation through fitting the daily zonally averaged data with assumed altitude and latitude variation of diurnal tide (1,1) mode. McLandress et al. (1996) obtained similar results for the diurnal tide latitude and altitude distribution based on UARS WINDII data, though limited between the 40° S and 40° N latitudes.

The upper right panel shows the semidiurnal tide amplitude and lower right is for the semidiurnal tide phase. In the northern hemisphere the semidiurnal tide amplitude peaks around 45° N. The least square fit amplitude is about 40 ± 5 m/s. In the southern hemisphere, we notice a peak at about 50° S (50 ± 10 m/s). UARS HRDI results (Burrage et al., 1995a) showed similar results in northern hemisphere, which were limited to 95 km altitude. It should be pointed out that TIDI is the first instrument that is able to show fairly extended latitude and altitude map for the semidiurnal tide amplitude and phase. It is not a surprise to see the peak amplitudes appear at latitudes shown in the TIDI data. The major semidiurnal tide modes (2,2), (2,3), and (2,4) all peak in the mid-latitudes, where the diurnal tides are very weak due to singularity in the tidal equations. The mode (2,3) peaks closest to the observed peak location. The vertical wavelengths for the semidiurnal tide mode are long. TIDI data appear to confirm that with very slow vertical variation of the phase. The northern hemisphere semidiurnal tide appears to have a vertical wavelength of ~50 km, while in the southern hemisphere it is longer. The semidiurnal tide (2,3) mode has a vertical wavelength about 80 km and (2,4) 50 km. The TIDI results are not far from these values.

Comparisons with the GSWM00 model output

Tidal wave modeling effort has been on going for some time. The NCAR/HAO Global Scale Wave Model (GSWM) has gone through many improvements (Hagan et al., 1995; 1999; Hagan and Roble 2001). The latest GSWM02 (Hagan and Forbes, 2002; 2003) also include the effect of the tropospheric latent heat release and non-migrating tide components. For our purposes, we used GSWM00 (Hagan and Roble, 2001), which includes migrating diurnal and semidiurnal tides. The GSWM00 results are readily available on the web. We plotted the migrating diurnal and semidiurnal tides for the month of April in Figure 5 in the same format as TIDI data in Figure 4 for easy comparison. The northern hemisphere amplitude is comparable with that from the TIDI observation. The southern hemisphere amplitude is much stronger than that shown by the TIDI data. The peak altitude in the GSWM00 is higher than (between 100 and 105 km) that from the TIDI (between 95 and 100 km). Though not clearly shown here, the vertical wavelength (~25 km) from the GSWM00 is also longer than that from the TIDI results (~20 km). It should be noted that McLandress et al. (1996) also showed that the UARS observed peak altitude was also lower than the model prediction from the GSWM95 (Hagan et al., 1995).

The semidiurnal tide from the GSWM00 show strong peaks centered at 45°S and 45°N, which are at similar locations where the TIDI data peaked. The peak altitudes in the model are also higher than observed by TIDI. The model peak amplitude is stronger than the TIDI results. The vertical wavelength for the semidiurnal tide in the northern hemisphere is close to that of TIDI observation. In the southern hemisphere, the vertical wavelength is also comparable with TIDI results.

Since the yaw period also cover part of March and May, it is useful to describe briefly the GSWM00 results for these two months. In March the diurnal tide is slightly weaker than April with peak amplitude about 50 m/s and the semidiurnal tide are stronger with a 75 m/s peak in the southern hemisphere and 60 m/s peak in the north. In May, the diurnal tide amplitude is about the same as in April; the semidiurnal tide is weaker than that in April with a 50 m/s peak near 105 km in the southern hemisphere and a similar size peak in the northern hemisphere at altitudes higher than 110 km. The GSWM00 shows that the

diurnal tide did not change much, while the semidiurnal tide experience a decrease in amplitude over the yaw period.

Comparison with Ground-based meteor radar

In the past satellite measurements of neutral winds have been compared with ground-based observations with mixed results (Burrage et al., 1996). Some ground-based measurements agreed with the satellite measurements better than others. Meridional wind component tends to have better agreement than the zonal component and the cause is still a mystery (Forbes et al., 2004). Nevertheless, such comparisons are necessary for both the ground-based instruments and satellite observations, because they can help improve the data processing procedures for both sides. For this analysis, we selected the ground-based meteor radar from Maui (20°N) for comparison. The radar was selected for the following reasons: 1) it provides 24-hour coverage; 2) its location is where the diurnal tide peaks, thus it can provide large range for the wind; 3) the meteor is co-located with a sodium lidar and the radar results have been cross-calibrated with the lidar (Franke et al., 2004). Figure 6 shows the meridional winds from meteor radar on March 1, 2004. A strong diurnal oscillation is clearly visible in meridional component. Since the TIDI instrument warmside (we use only warmside for the northern hemisphere) sample only two local times each day, we selected the meteor data according to the TIDI overpass times on each day during the yaw period (day 2004/03/19-05/19) and composed the multi-day sampled 24-hour local time data set for the TIDI comparison. The meridional winds from the radar and TIDI are plotted in Figure 7. Not surprisingly both the radar meridional (upper panel) and TIDI meridional winds (lower panel) show the similar positive and negative bands with a slope matching a diurnal variation. There appear to be a small vertical offset between the two data sets. Overall, the two data sets show a reasonable agreement.

Summary

In this report, we analyzed zonally averaged TIDI meridional wind data from one yaw period 2004/03/19 to 2004/05/19 near equinox. The multi-day data set provides 24-hour local time coverage, which allows the extraction of diurnal and semi-diurnal tides. The TIDI data provided good latitudinal and altitudinal coverages of the migrating diurnal and semidiurnal tide amplitude and phase. The TIDI results are compared with GSWM00 output for the month of April. The TIDI diurnal tide results agree with the GSWM00 output very well in the northern hemisphere and differ in amplitude in the southern hemisphere. Other differences are subtler. For example the diurnal tide amplitude peaked at an altitude lower than the model predicted by 5 km. The diurnal tide vertical wavelength for the TIDI results also a bit shorter than that shown in the model. The TIDI data can help to refine the model parameters in the future. The semidiurnal tide results are also encouraging. The TIDI results do resemble the model output in some aspects. For example, the both appear to show the semidiurnal tide peaks at 45° latitude. The comparison with ground-based meteor radar shows reasonable good results. Other studies with TIDI neutral winds are on going, we will report more results in the near future.

Acknowledgments

This research is supported by NASA grant NAG5-5334 to the National Center for Atmospheric Research (NCAR) and grant NAG5-5049 to the University of Michigan. NCAR is supported by the National Science Foundation. The Maui meteor radar operation is supported by National Science Foundation grants ATM 00-03182 and ATM 00-3198. Many helpful comments from Dr. Maura Hagan are greatly appreciated.

References

Burrage, M. D., D. L. Wu, W. R. Skinner, D. A. Ortland, and P. B. Hays, 1995a, Latitude and seasonal dependence of the semidiurnal tide observed by the high resolution Doppler imager, *J. Geophys. Res. 100*, 11313-11321.

Burrage, M. D., M. E. Hagan, W. R. Skinner, D. L. Wu, and P. B. Hays, 1995b, Long-term variability in the solar diurnal tide observed by HRDI and simulated by the GSWM, Geophys. Res. Lett., 22, 2641-2644.

Burrage, M. D., W. R. Skinner, D. A. Gell, P.B. Hays, A. R. Marshall, D. A. Ortland, A. H. Manson, S. J. Franke, D. C. Fritts, P. Hoffman, C. McLandress, R. Niciejewski, F. J. Schmidlin, G. G. Shepherd, W. Singer, T. Tsuda, and R. A. Vincent, 1996, Validation of mesosphere and lower thermosphere winds from the high-resolution Doppler imager on UARS, *J. Geophys. Res., 101*, 10,365-10,392.

Chapman, S. and R. S. Lindzen, 1970, *Atmospheric tides*, Gordon and Breach, pp. 200, Newark, NJ.

Forbes, J. M., 1982a, Atmospheric tides, 1, Model description and results for the solar diurnal component, *J. Geophys. Res., 87*, 5222-5240.

Forbes, J. M., 1982b, Atmospheric tides, 2, The solar and lunar semidiurnal components, *J. Geophys. Res., 87*, 5241-5252.

Forbes, J. M. and M. E. Hagan, 1988, Diurnal propagating tide in the presence of mean winds and dissipation: A numerical investigation, *Planet. Space Sci., 36*, 579-590.

Forbes, J. M., Yu. I. Portnyagin, W. Skinner, R. A. Vincent, T. Solovjova, E. Merzlyakov, T. Nakamura, and S. Palo, 2004, Climatological lower thermosphere winds as seen by ground-based and space-based instruments, *Ann. Geophy., 22*, 1931-1945.

Franke, S. J., X. Chu, A. Z. Liu, W. K. Hocking, Comparison of meteor radar and Na Doppler lidar measurements of winds in the meospause region above Maui, HI, submitted to J. Geophys. Res., 2004.

Hagan, M. E., J. M. Forbes, and F. Vial, 1995, On modeling migrating solar tides, *Geophys. Res. Lett, 22*, 893-896.

Hagan, M. E. M. D. Burrage, J. M. Forbes, J. Hackney, W. J. Randel, and X. Zhang, 1999, GSWM-98: Results for migrating solar tides, *J. Geophys. Res., 104*, 6813-6827.

Hagan, M. E. and R. G. Roble, 2001, Modeling diurnal tidal variability with the National Center for Atmospheric Research thermosphere-ionosphere-mesosphere-electrodynamics general circulation model, *J. Geophys. Res., 106*, 24,869-24,882.

Hagan, M. E. and J. M. Forbes, 2002, Migrating and nonmigrating diurnal tides in the middle and upper atmosphere excited by tropospheric latent heat release, *J. Geophys. Res.,107*, doi:10.1029/2001JD001236.

Hagan, M. E. and J. M. Forbes, 2003, Migrating and nonmigrating semi-diurnal tides in the upper atmosphere excited by tropospheric latent heat release, *J. Geophys. Res.,108*, doi:10.1029/2002JA009466.

Hays, P. B., T. L. Killeen, and B. C. Kennedy, 1981, The Fabry-Perot Interferometer on Dynamics Explorer, *Space Sci. Instrum., 5*, 395-416.

Hays, P. B., V. J. Abreu, M. E. Dobbs, D. A. Gell, H. J. Grassl, and W. R. Skinner, 1993, The High Resolution Doppler Imager on the Upper Atmospheric Research Satellite, *J. Geophys. Res., 98*, 10,713-10,723.

Hays, P. B., D. L. Wu, M. D. Burrage, D. A. Gell, H. J. Grassl, R. S. Lieberman, A. R. Marshall, Y. T. Morton, D. A. Ortland, W. R. Skinner, 1994, Observations of the diurnal tide from space, *J. Atmos. Sci*. *51*, 3077-3093.

Hays, P. B., 1990, Circle to line interferometer optical system, *Applied Optics, 29***,** 1482-1489.

Huang, F. T. and C. A. Reber, 2003, Seasonal behavior of the semi-diurnal tides and mean flows at 95 km, based on measureuments from the High Resolution Doppler Imager (HRDI) on the Upper Atmospheric Research Satellite (UARS), J. Geophys. Res., 108, doi:10.1029/2002JD003189.

Khattatov, B. V. V. A. Yubin, M. A. Geller, P. B. Hays, R. A. Vincent, 1997a, Diurnal migrating tide as seen by the high resolution Doppler imager/UARS 1. Monthly mean global meridional winds, *J. Geophys. Res., 102*, 4405-4422.

Khattatov, B. V., M. A. Geller, V. A. Yubin, P. B. Hays, 1997b, Diurnal migrating tide as seen by the high resolution Doppler imager/UARS 2. Monthly mean global zonal and vertical velocities, pressure, temperature, and inferred dissipation, *J. Geophys. Res*., *102***,** 4423-4435.

Killeen, T. L. and P. B. Hays, 1982, Doppler line profile analysis for a multi-channel Fabry-Perot interferometer, *Appl. Opt*., *23*, 612-620.

Killeen, T. L., W. R. Skinner, R. M. Johnson, C. J. Edmonson, Q. Wu, R. J. Niciejewski, H. J. Grassl, D. A. Gell, P. E. Hanson, J. D. Harvey, J. F. Kafkalidis, 1999, TIMED Doppler Interferometer (TIDI), *Proc. SPIE* 3756, 289-301, Optical Spectroscopic Techniques and Instrumentation for Atmospheric and Space Research III, Allen M. Larar Ed.

Lieberman, R. S. and P. B. Hays, 1994, An estimate of the momentum deposition in the lower thermosphere by the observed diurnal tide, *J. Atmos. Sci., 51*, 3094-3105.

McLandress, C., G. G. Shepherd, and B. H. Solheim, 1996, Satellite observations of thermospheric tides: Results from the Wind Imaging interferometer on UARS, *J. Geophys. Res., 101*, 4093-4114.

Morton, Y. T. R. S. Lieberman, P. B. Hays, D. A. Ortland, A. R. Marshell, D.L. Wu, W. R. Skinner, M. D. Burrage, D. A. Gell, and J. –H. Yee, 1993, Global meosospheric tidal winds observed by the high resolution research satellite, *Geophys. Res. Lett., 20*, 1263-1266.

Pancheva, D, E. Merzlyakov, N. J. Mitchell, Y. Portnyagin, A. H. Manson, C. Jacobi, C. E. Meek, Y. Luo, R. R. Clark, W. K., Hocking, J. MacDougall, H. G. Muller, D. Kurschner,G. O. L. Jones, R. A. Vincent, I. M. Reid, W. Singer, K. Igarashi, G. I. Fraser, A. N. Fahrutdinova, A. M. Stepanov, L. M. G. Poole, S. B. Malinga, B. L. Kashcheyev, A. N. Oleynikov, 2002, Global-scale tidal variability during the PSMOS campaign of June-August 1999: interaction with planetary waves, *J. Atmos. Sol.-Terr. Phys., 64***,** 1865-1896.

Shepherd, G. G., G.Thuillier, W. A. Gault, B. H. Solheim, C. Herscom, J. M. Alunni, J. F. Brun ,S. Brune, P. Charlot, L. L. Cogger, D. L. Desaulniers, W. F. J. Evans, R. L. Gattingerm, F. Girod, D. Harvie, R. H. Hum, D. J. W. Kendall, E. J. Llewellyn, R. P. LOWE, J. Ohrt, F. Pasternak, O. Peillet, I. Powell,

Y. Rochon, W. E. Ward, R. H. Wiens, J. Wimperis, 1993**,** WINDII, The WIND Imaging Interferometer on the Upper-Atmosphere Research satellite, *J. Geophys. Res*. *98*, 10,725-10,750.

Skinner, W. R., R. J. Niciejewski, T. L. Killeen, S. C. Solomon, R. D. Gablehouse, Q. Wu, D. Ortland, D. A. Gell, A. R. Marshall, E. Wolfe Jr., M. Cooper, J. F. Kafkalidis, 2003, Operational Performance of the TIMED Doppler Interferometer (TIDI), *Proc*. *SPIE, 5157*, 47-57.

Vial, F., 1989, Tides in the middle atmosphere, *J. Atmos. Terr. Phys*., *51*, 3-17.

Figure Captions

Figure 1. Local time and latitude coverage during day 2004/03/20 (day 80) at 85 km altitude. The red (blue) is for the warmside (coldside). The open (closed) symbols are for the daytime (nighttime) sector. The single black arrow point toward the satellite flying direction. The two-head arrows mark the segments of the data where warmside (coldside) for the northern (southern) hemisphere provides nearly similar local time from the equator to the pole. These data segment are later used in the analysis.

Figure 2. Zonally averaged meridional winds from the coldside (left) and warmside (right). Inside each panel, the ascending node is on the left and descending node is on the right. The ascending node on this day was in the nighttime and descending node in the daytime. The black arrows in the panels mark the same data segments highlighted in Figure 1. These segments are later used for the tidal analysis.

Figure 3. Meridional winds during one yaw period from three northern latitudes. The data from 11.29, 30.36, and 44.79 latitudes are shown from upper to lower panels. The rightside (12-24 LT) is from ascending node and leftside (0-12 LT) is from the descending node. At the beginning of the yaw period (day 2004/03/19) the ascending node is near midnight and as the day progresses and local time for sampling moves backward toward earlier hours. Near the end of the yaw period (day 2004/05/19), the ascending node has moved from midnight to near local noon. The descending node starts near local noon and moves backward to the midnight at the end of the yaw period. It should be noted that the warmside will never sample the midnight sector because of the yaw maneuver. At the same time, the coldside will never sample the local noon sector.

Figure 4. Least squares fit results of diurnal and semidiurnal tide amplitude and phase. The least squares fits with a background wind, a diurnal oscillation, and semidiurnal oscillation are performed for data taken at different latitudes and altitudes. The diurnal tide amplitude (upper left) and phase (lower left) are displayed. The semidiurnal amplitude (upper right) and phase (lower right) are also shown. The northern (southern) hemisphere results are from the warmside (coldside).

Figure 5. The GSWM00 output of diurnal and semidiurnal tide amplitude and phase for the month of April. The plot is in the same format as Figure 4.

Figure 6. Meteor radar meridional wind data on March 1, 2004.

Figure 7. Multi-day composite of local time variation of the meridional wind for the yaw period (2004/03/19-2004/05/19) from Maui meteor radar. During this yew period, TIDI warmside pass over Maui twice a day (on ascending and descending nodes separated by about 12 hours), the Maui data were selected according to these overpass times and combined to form this data set for comparison with TIDI data. TIDI measurements of the meridional wind at 20° N are shown in the lower panel.

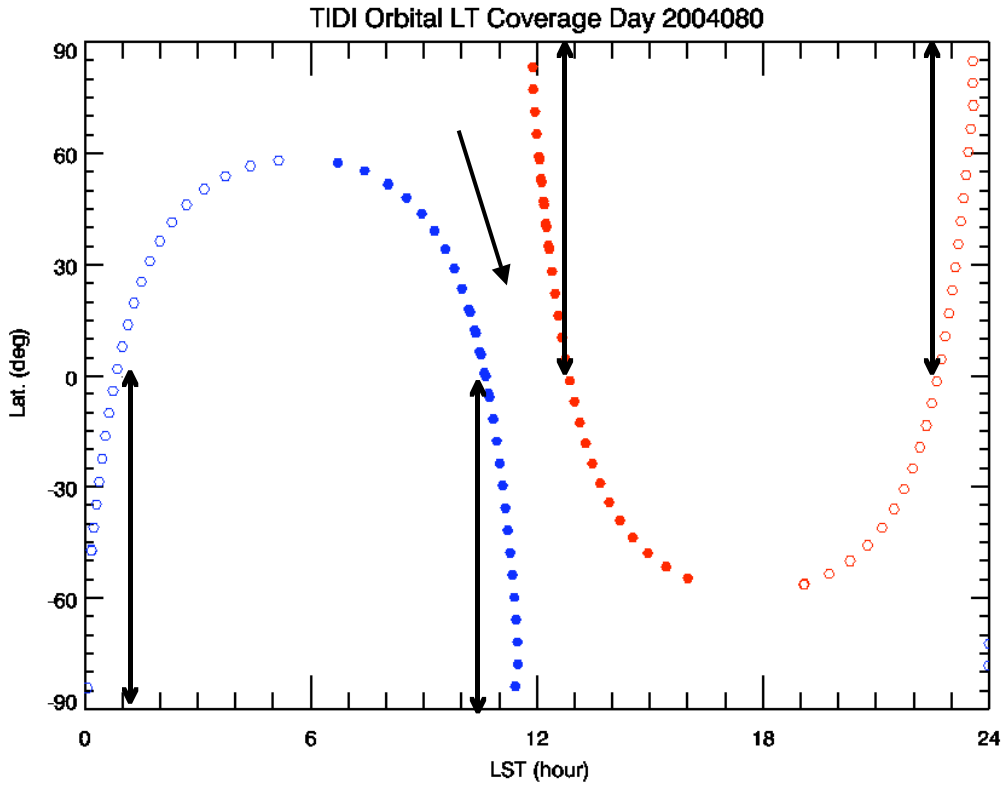

Figure 1.

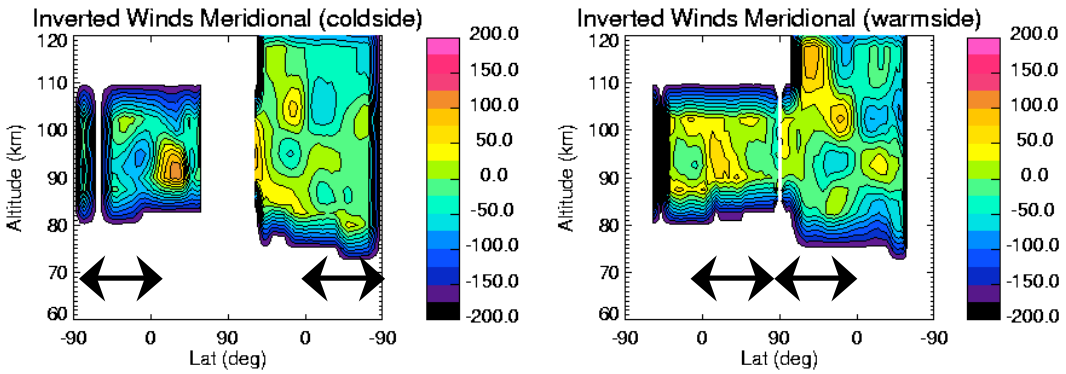

Figure 2.

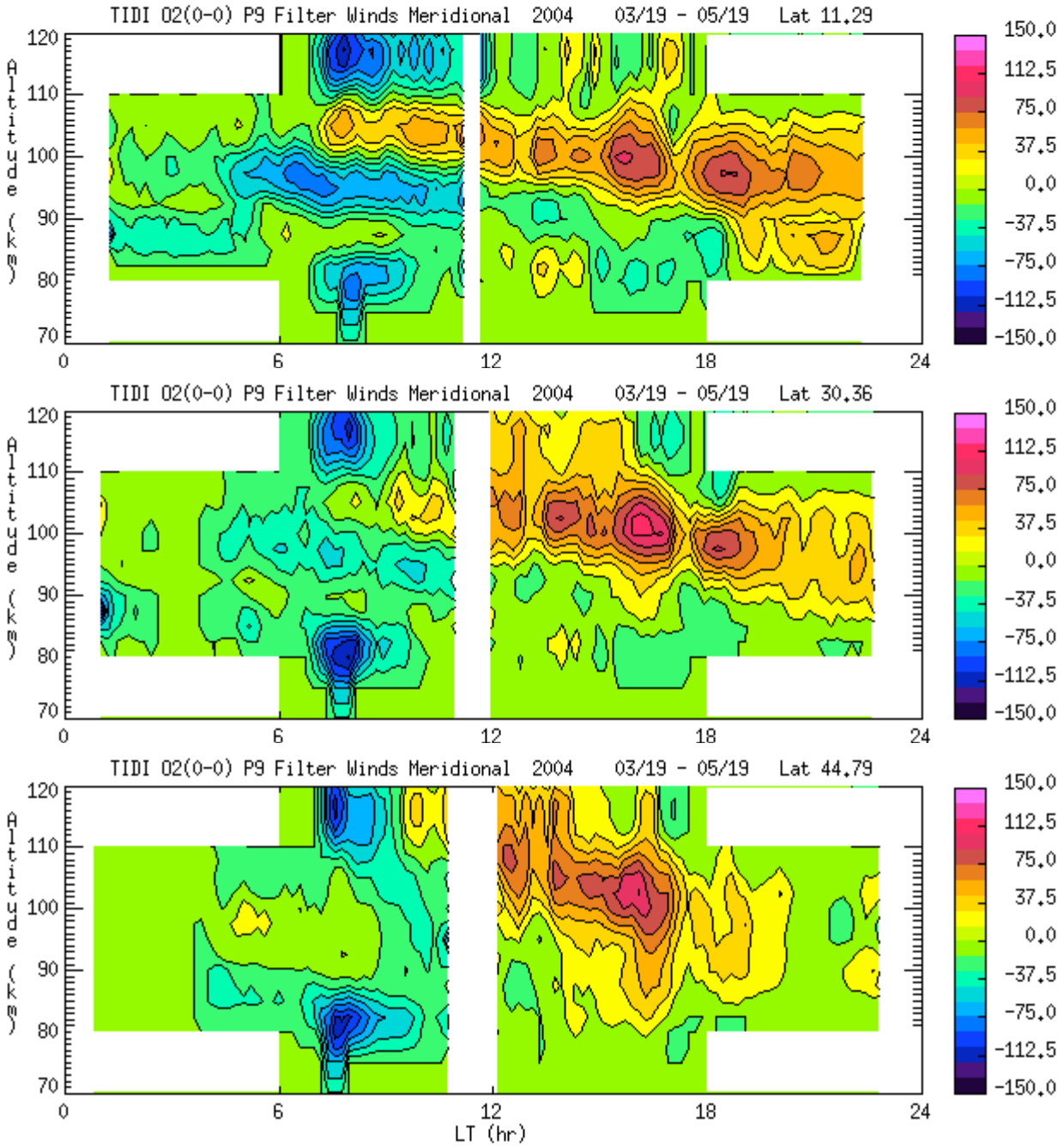
TIDI O2(0-0) P9 Filter Winds Meridional 2004 03/19 - 05/19 Lat 11.29
TIDI O2(0-0) P9 Filter Winds Meridional 2004 03/19 - 05/19 Lat 30.36
TIDI O2(0-0) P9 Filter Winds Meridional 2004 03/19 - 05/19 Lat 44.79
Altitude (km)
120
110
100
90
80
70
0
6
12
18
24
LT (hr)
150.0
112.5
75.0
37.5
0.0
-37.5
-75.0
-112.5
-150.0

Figure 3.

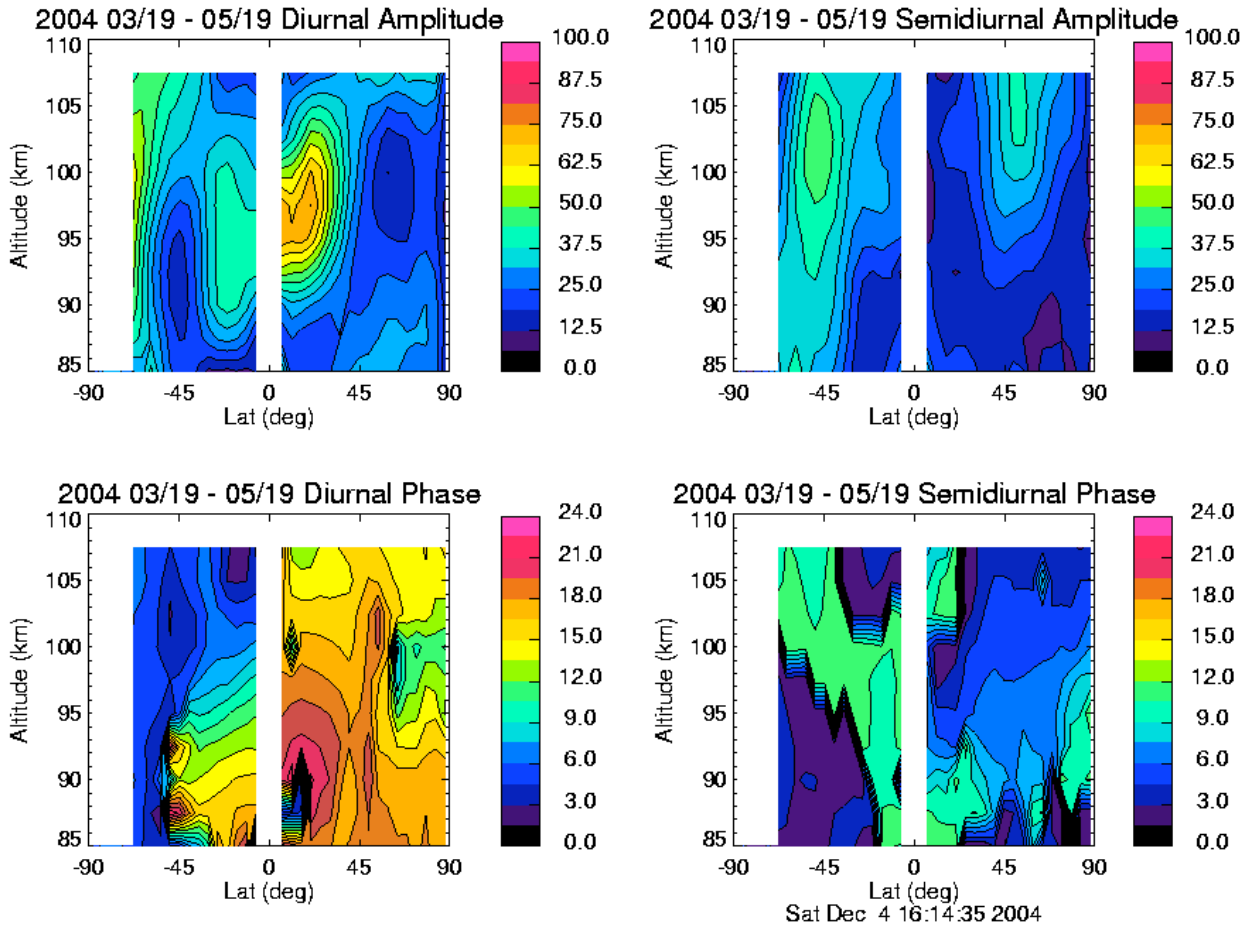
2004 03/19 - 05/19 Diurnal Amplitude
2004 03/19 - 05/19 Semidiurnal Amplitude
2004 03/19 - 05/19 Diurnal Phase
2004 03/19 - 05/19 Semidiurnal Phase
Altitude (km)
Lat (deg)
110
105
100
95
90
85
-90
-45
0
45
90
100.0
87.5
75.0
62.5
50.0
37.5
25.0
12.5
0.0
24.0
21.0
18.0
15.0
12.0
9.0
6.0
3.0
0.0
Sat Dec 4 16:14:35 2004

Figure 4.

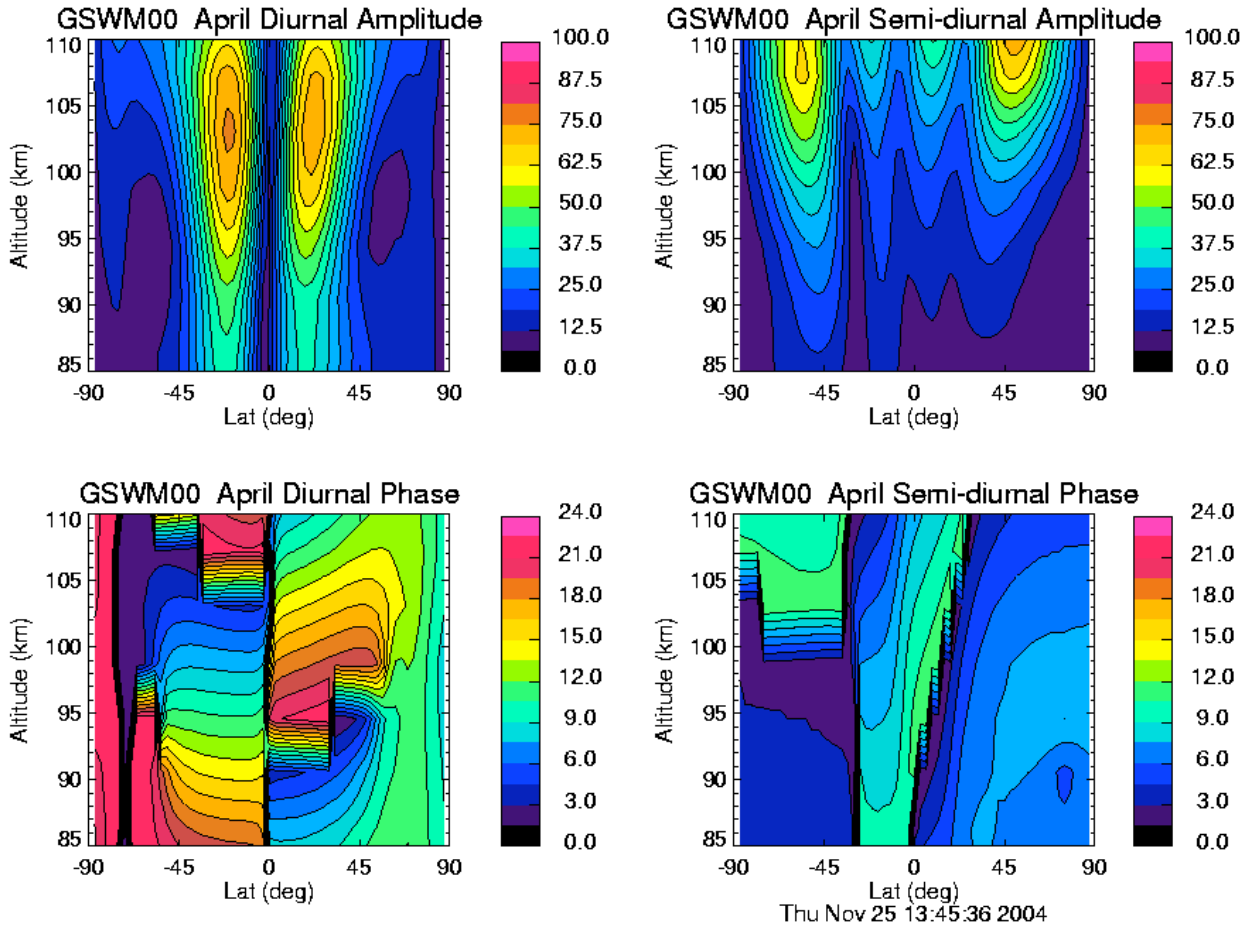

Figure 5.

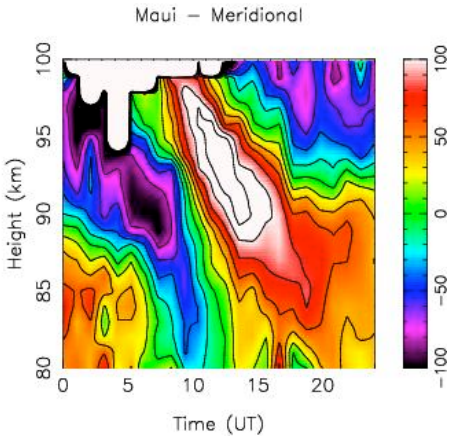

Figure 6.

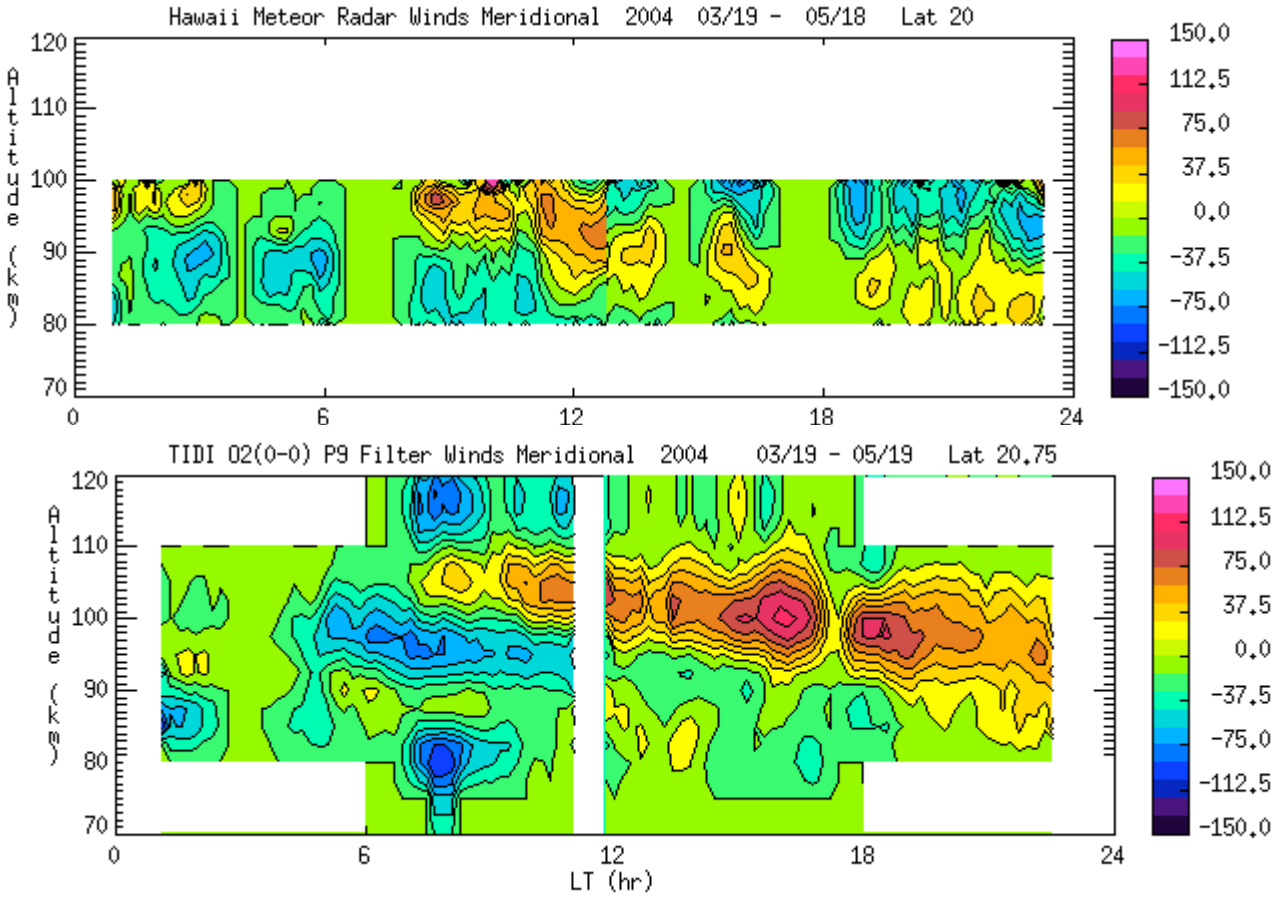
Hawaii Meteor Radar Winds Meridional 2004 03/19 - 05/18 Lat 20
Altitude (Km)
120
110
100
90
80
70
0
6
12
18
24
150.0
112.5
75.0
37.5
0.0
-37.5
-75.0
-112.5
-150.0
TIDI 02(0-0) P9 Filter Winds Meridional 2004 03/19 - 05/19 Lat 20.75
Altitude (Km)
LT (hr)

Figure 7